Microgravity Science and Technology (2019) 31:381–393
https://doi.org/10.1007/s12217-019-9697-y

ORIGINAL ARTICLE

Numerical Investigation on Single Bubble and Multiple Bubbles Growth and Heat Transfer During Flow Boiling in A Microchannel Using the VOSET Method

Kaikai Guo[1] · Huixiong Li[1] · Yuan Feng[1] · Jianfu Zhao[2,3] · Tai Wang[4]

Received: 2 February 2019 / Accepted: 2 April 2019 / Published online: 17 April 2019

Abstract
With the rapid development of modern space technologies, heat sinks with high heat flux have become a bottleneck in the development of high capacity electronic equipment with high power densities. To ensure the stability and security of heat sink devices, it's crucial to greatly enhance the heat transfer performance of the heat sink device and flow boiling in microchannels has attracted more and more attention due to its unique advantages. The objective of this investigation is to study the growth and heat transfer of single bubble and multiple bubbles during flow boiling in a microchannel using the VOSET method. In order to verify the accuracy of the numerical model adopted in this paper, the results obtained by the present method were compared with that of previous experiments and numerical calculations. After that, effects of Re and wall superheat on the bubble morphologies and heat transfer in a microchannel were studied. Increasing Reynolds number could increase the bubble growth rate and boiling flow heat transfer. However, there was a slight increase in heat transfer performance with an increase in wall superheat. In addition, when Re reached a certain value, the elongated bubble zone would appear in the microchannel. Further, the stretching length, the contact length between the heated wall and the vapour and the second kind of thin liquid layer were analyzed in detail. Finally, more importantly, the dynamics and heat transfer of multiple bubbles with different bubble waiting time were presented. With a decrease in bubble waiting time, the heat transfer performance was enhanced significantly.

Keywords Single bubble · Multiple bubbles · Flow boiling · Microchannel · VOSET Method

Introduction

With the rapid development of modern space technologies, heat sinks with high heat flux have become a bottleneck in the development of high capacity electronic equipment with high power densities. The high power is concentrated on the small device area, which greatly increases the heat flux. The heat flux will be expected to reach 1000 W/cm^2 in the near future (Krishnan et al. 2007). In order to ensure the stability and reliability of the heat dissipation device, it is very important to improve its heat transfer performance. The microchannel cooling technology has attracted more and more attention because of its strong heat transfer performance, compactness, heat transfer uniformity and other advantages. The microchannel cooling technology can be used in various fields, such as gas turbine blade cooling, data center cooling, rocket nozzle cooling, and micro-chemical engineering (Kim and Mudawar 2014). In the past few years, the single-phase flow cooling technology in microchannels has been applied in the market (Hussien et al. 2016). Many data centers have started to adopt the single-phase flow cooling technology in microchannels to reduce the operating temperature of devices. However, the single-phase flow in the microchannel will lead to the problem of high local temperature, which will cause greater thermal stress. Based on the phase change heat transfer mechanism, the microchannel flow boiling cooling can reduce

✉ Huixiong Li
huixiong@mail.xjtu.edu.cn

[1] State Key Laboratory of Multiphase Flow in Power Engineering, Xi'an Jiaotong University, Xi'an 710049, People's Republic of China

[2] CAS Key Laboratory of Microgravity, Institute of Mechanics, Chinese Academy of Sciences (CAS), Beijing 100190, People's Republic of China

[3] School of Engineering Science, University of Chinese Academy of Sciences, Beijing 100190, People's Republic of China

[4] School of Energy Power and Mechanical Engineering, North China Electric Power University, Baoding 071003, People's Republic of China

the unevenness of temperature distribution and further reduce the heat transfer resistance. In addition, the averaged mass flow rate of the microchannel flow boiling system is smaller than that of the single-phase flow circulation system of the microchannel, which can greatly reduce the power requirement of the driving system. Now, more and more heat exchange equipment have restrictions on the friction power, forcing designers to reduce the mass flow rate. Microchannels have been also widely used in microgravity conditions (Arias et al. 2008; Ma et al. 2018). Under the space microgravity, the buoyancy force caused by gravity disappears, and the flow boiling phenomenon and heat transfer mechanism in the conventional channel are different from those on the earth. In the references (Konishi and Mudawar 2015; Dhir et al. 2012), the scholars pointed to the danger of enormous bubbles due to the absence of an effective force to make the bubble escape from the heated wall. In microgravity, there is the danger of unexpected occurrence of CHF at relatively low heat fluxes because of the formation of the enormous bubbles (Wan and Zhao 2008). However, the effect of the gravity on the bubble growth and heat transfer of the microchannel is negligible (Baldassari and Marengo 2013). The microchannel flow boiling cooling technology can avoid such problem. Therefore, the microchannel flow boiling cooling technology has attracted more and more attention due to its unique advantages (Agostini et al. 2007; Kuznetsov and Shamirzaev 2009; Wu et al. 2015).

In the past few decades, many scholars have made great progress in studying the boiling flow and heat transfer characteristics in the microchannel by means of experiments and numerical simulation (Karayiannis and Mahmoud 2017; Guo et al. 2014; Wang and Wang 2014; Tibiriçá and Ribatski 2013). Kattan et al. (1998a, 1998b, 1998c) studied flow patterns in conventional channels. They argued that flow patterns must be considered in order to better understand the thermophysical processes in the microchannel. However, Flow patterns that appear in regular channels may not exist in microchannels. For example, the capillary force in a microchannel can prevent the emergence of stratified flow, and the bubble flow in a conventional channel does not exist in the microchannel if a bubble fills the entire microchannel section. Therefore, the flow pattern in the microchannel will be different from that of conventional channel due to the influence of channel size. Kandlikar (2002) and Thome (2004) made a good summary of the research on flow boiling flow patterns in microchannels. They classified the boiling flow in the microchannel as isolated bubby flow, elongated bubby/slug flow and annular flow. Thome et al. (2004; Thome et al. 2004) proposed a three-zone model to predict the heat transfer in a microchannel based on the premise that the evaporation heat transfer of thin liquid film is the main heat transfer mechanism. The three zones in this model are liquid slug, evaporating elongated bubble and vapor slug. They demonstrated that the high heat flux during boiling in a microchannel lies in the thin liquid film around the elongated bubble. Balasubramanian and Kandlikar (2005) conducted an experimental study on boiling flow in microchannels. The process of forming a bubble to become a plug was observed in the experiment. In addition, they provided pictures of bubbles growing during the experiment, in which a liquid film formed between the bubbles and the wall during the growing process.

It can be seen from the above literatures that, the bubbles in the microchannel will fill the entire channel section after a certain degree of growth and elongation along the flow direction to form the elongated bubbles due to the influence of the size of the microchannel. During the stretching process, a thin liquid film formed between the elongated bubble and the heating wall surface. Harirchian and Garimalla (2010) believed that an important mechanism of boiling in the microchannel was that a thin liquid film would be formed near the heated wall during stretching of the bubbles. Mukherjee et al. (2011) also believed that the shape of the elongated bubbles had an important influence on the heat transfer characteristics of the microchannel. Therefore, the study on the growth of the elongated bubbles will help us better understand the heat transfer mechanism of flow boiling in microchannels. Hub et al. (2007) studied the growth of the elongated bubbles in microchannels and the influence of the elongated bubbles on flow boiling using two methods of numerical calculation and experimental observation. They believed that the elongated bubble flow is a unique flow pattern in microchannel flow boiling. The development of flow patterns and heat transfer characteristics are closely related to the morphology of the elongated bubbles. The growth behavior of the elongated bubbles is mainly dominated by evaporation of thin liquid film. Agostini et al. (2008) studied the variation of velocity of the elongated bubbles in microchannels, and proposed the prediction model. New data obtained by Revellin et al. (2008) showed that 92% of the data fell within the error band of plus or minus 20% of the above prediction model. Arcanjo et al. (2010) presented visual observation on the flow pattern of the flow boiling in the microchannel and measured the velocity, frequency and length of the elongated bubbles. They classified flow patterns as bubbly flow, elongated bubbles flow, churn flow and annular flow. Besides, they also found that the velocity of the elongated bubbles was mainly influenced by the mass velocity, the vapor quality, and the saturation temperature in the microchannel. The velocity of the elongated bubbles increases with an increase in the mass velocity and vapor quality, however decreases with an increase in the saturation temperature. Mukherjee and Kandlikar (2005) used the level-set method to simulate the growth of a single bubble in an overheated medium in a microchannel. Their results showed that the

bubble maintains a basically stable growth rate at the initial stage of growth. However, when the bubble size is almost the same as the size of the microchannel section, the bubble is gradually stretched along the axial direction. Besides, a thin liquid layer between the wall surface and the bubble interface is formed. They found that there was a large heat transfer rate in the thin liquid layer near the three-phase contact line and the growth rate of bubbles increased significantly due to the existence of thin liquid layer. Then Mukherjee described this interpretation in more detail in another literature (Mukherjee 2009). Lee and Son (2008) developed a simplified model of microlayer and combined level-set method to conduct a numerical simulation study on the boiling flow of a single bubble in a rectangular microchannel. When the size of the channel is smaller than the departure diameter of the bubble, the growth rate and heat transfer rate of the bubble increase significantly. Moreover, they found that the microlayer between the bubble and the channel's corners had a significant impact on overall heat transfer performance. They also found that as the forward contact angle and the backward contact angle decreased, the heat transfer rate increased and the backward contact angle became more significant. Magnini et al. (2013a, 2013b) simulated the boiling flow in the cylindrical microchannel with the help of the commercial software FLUENT. They simulated the growth of a single bubble and two bubbles on the central axis of the channel, and modified the three-region model of microchannel boiling heat transfer proposed by Thome et al. (2004) based on the simulation results, and proposed a new prediction model. Ling et al. (2015) used VOSET method to conduct numerical simulation on bubble growth and merge in microchannel boiling flow. When the bubble grows along the wall, the heat flux is mainly concentrated on the liquid side near the three-phase contact line. The bubble merge in the microchannel will temporarily improve the heat flux of the wall, but the high heat flux of the boiling flow in the microchannel is mainly attributed to the liquid film near the three-phase contact line. Jafari and Okutucu-Özyurt (2016) simulated the flow boiling in the microchannel using COMSOL software and Cahn-Hilliard phase field method. They set up a microcavity near the entrance of the channel, which continuously produced bubbles. They studied the nucleation and growth of the bubble, and the distribution of the velocity, temperature and pressure of the released bubbles was also obtained. In their results, the heat transfer rate decreases rapidly along the flow direction because there is no microlayer between the bubble and the wall. Katiyar et al. (2016) and Luo et al. (2017) respectively adopted level-set method and VOF method to analyze the influencing factors of the single bubble in microchannel boiling flow. They studied the effects of static contact Angle, surface tension, wall overheat and Reynolds number on bubble growth and heat transfer.

Based on the above literature results, the growth of the elongated bubble has an important influence on the heat transfer characteristics of the flow boiling in microchannels. However, there is not enough research on the elongated bubbles in the flow boiling in the microchannel. In the studies of Mukherjee and Kandlikar (2005), Lee and Son (2008), Ling et al. (2015), Jafari and Okutucu-Özyurt (2016) and Katiyar et al. (2016), there is no elongated bubble zone mentioned by Thome (2004) in the microchannel due to the low Reynolds number. It can be seen that there is a certain condition for the appearance of the elongated bubble zone. In addition, the formation morphology of the elongated bubble in microchannels are also different under different Reynolds number and wall superheat conditions, which will have different effects on heat transfer. Therefore, it is very important to study the growth of the elongated bubble under different Reynolds number and wall superheat conditions. Finally, the dynamics and heat transfer characteristics of multiple bubbles are different with that of single bubble and there is less relevant research. Based on the above considerations, the growth and heat transfer mechanism of single bubble and multiple bubbles in microchannels are further analyzed by means of the numerical calculation method in this paper. The formation conditions of the elongated bubble zone in the microchannel and the influence of Reynolds number and wall superheat on the growth and heat transfer characteristics of the bubble will help us better understand the mechanism of the flow boiling in the microchannel. The study on the dynamics and heat transfer characteristics of multiple bubbles will also provide a reference for improving the heat transfer performance of microchannels.

Numerical Modelling

Governing Equation

Due to the existence of the phase change, the expressions of the two-phase flow governing equations for the boiling are different from that of single flow, which can be written as:

$$\nabla \cdot u = \dot{m}\left(\frac{1}{\rho_g} - \frac{1}{\rho_l}\right) \tag{1}$$

$$\rho\left(\frac{\partial \boldsymbol{u}}{\partial t} + \boldsymbol{u}\cdot\nabla\boldsymbol{u}\right) = -\nabla p + \nabla\cdot\left[\eta\left((\nabla\boldsymbol{u}) + (\nabla\boldsymbol{u})^{T}\right)\right] + \rho\boldsymbol{g}(1-\beta_{T}(T-T_{sat})) + \boldsymbol{F}_{s} \tag{2}$$

$$\frac{\partial T}{\partial t} + u\cdot\nabla T = \frac{k}{\rho C_p}\nabla^2 T \tag{3}$$

where ρ, $\boldsymbol{u}$, p, η, $\boldsymbol{g}$, T, k and C_p represent density, velocity, pressure, viscosity, gravitational acceleration, temperature, thermal conductivity and specific heat, respectively. $\dot{m}$ denotes

the mass transfer rate produced by the evaporation on the phase interface. β_T is the coefficient of volumetric expansion, T_{sat} is the saturation temperature of the liquid phase, The surface tension term $\boldsymbol{F}_s$ is written as a source term in the momentum equation using CSF model (Brackbill et al. 1992), which is expressed as

$$\boldsymbol{F_s} = -\sigma\kappa(\phi)\delta(\phi)\nabla\phi \tag{4}$$

where σ is surface tension coefficient, ϕ is level set function, $\kappa(\phi)$ is interface curvature and $\delta(\phi)$ is Dirac delta function. $\kappa(\phi)$ and $\delta(\phi)$ can be defined as follows.

$$\kappa(\phi) = \nabla\cdot\left(\frac{\nabla\phi}{|\nabla\phi|}\right) \tag{5}$$

$$\delta(\phi) = \begin{cases} 0 & \text{when } |\phi| > s \\ \dfrac{1}{2s}\left[1+\cos\left(\dfrac{\pi\phi}{s}\right)\right] & \text{when } |\phi| \le s \end{cases} \tag{6}$$

where s is the width of smooth areas between both sides of the phase interface, which is defined as $s = 1.5\ h$. h is grid size.

Solving Governing Equations

The governing equations are discretized by finite volume method based on collocated grid in the present study. The convection term adopts QUICK format, the diffusion term adopts the central difference format, and finally, the discrete equations are solved by the alternating direction implicit iteration method (ADI method). The unsteady IDEAL algorithm (Sun et al. 2008) is adopted to deal with the coupling of pressure and velocity.

In this paper, the temperature of the grid unit containing the phase interface is solved using Ling et al.'s processing method (Ling et al. 2015), as shown Fig. 1. For a grid unit containing a phase interface, the temperature is calculated using linear interpolation in the normal direction of the phase interface. If the center of the grid is located in the gas phase, interpolation

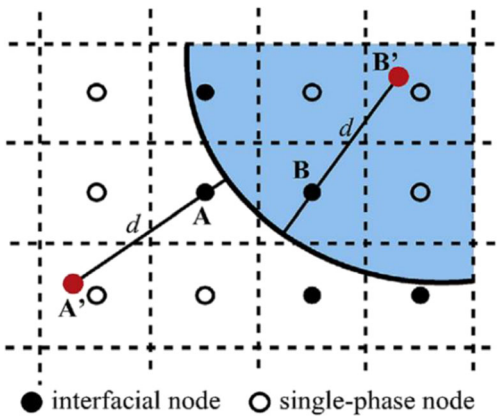

Fig. 1 The method solving the temperature field with an immersed boundary condition on the interface (Ling et al. 2015)

point A` is sought along the normal direction of the phase interface. The distance between point A` and grid center point A is 1.5 times grid size. The temperature of grid center point A is estimated according to the distance between these two points and the phase interface. If the center of the phase interface grid is located in the liquid phase, the temperature of this unit center B can be calculated using same method. The temperature at node A and B can be calculated using the following equation:

$$\frac{T_A - T_{sat}}{T_{A'} - T_{sat}}| = \frac{|\phi_A|}{|\phi_A| + d} \tag{7}$$

$$\frac{T_B - T_{sat}}{T_{B'} - T_{sat}}| = \frac{|\phi_B|}{|\phi_B| + d} \tag{8}$$

where d is 1.5 times grid size. The temperature of the point A` and B` are obtained by a bilinear interpolation from nearby cells. ϕ_A and ϕ_B are level set function of the cell A and B. Please see the literature of Ling et al. (2015) for the temperature solution details of grid cell containing phase interface.

Solving Interfacial Mass Transfer Rate

Assuming that dV is the volume of the control unit Ω and dA is the area of the gas-liquid interface Γ, the following relationship needs to be satisfied.

$$\int_\Omega \dot{m} dV = \frac{1}{\gamma}\int_\Gamma \dot{q} dA \tag{9}$$

where γ is latent heat of evaporation. $\dot{q}$ refers to the heat flux flowing into the interface, as shown:

$$\dot{q} = k_g \frac{\partial T}{\partial n}\bigg|_g - k_l \frac{\partial T}{\partial n}\bigg|_l \tag{10}$$

In this paper, a normal probe technique proposed by (Mukherjee et al. 2011) and bilinear interpolation method are used to calculate the temperature gradient on both sides of the phase interface. For the detailed solution process, please see the literatures (Ling et al. 2015; Udaykumar et al. 1999). The temperature gradient on both sides of the phase interface is obtained, then the mass transfer rate can be calculated by the following formula:

$$\int_\Omega \dot{m} dV = \frac{1}{\gamma}\left(k_g \frac{\partial T}{\partial n}\bigg|_g - k_l \frac{\partial T}{\partial n}\bigg|_l\right)\Delta A \tag{11}$$

where ΔA is the area of the phase interface of grid cell containing phase interface, which can be obtained by geometric method.

Interface Tracking

The VOSET method, a coupled VOF and Level set method proposed by Sun and Tao (2010), can not only calculate accurately the

physical quantity near the interface such as surface tension, but also maintain good conservation of the mass. Compared with the CLSVOF method, the VOSET method is more concise and easy to implement. For details of the treatment of the VOSET method, please refer to the literatures (Sun and Tao 2010; Wang et al. 2014).

Taking the phase change into consideration, the VOF equation can be written as

$$\frac{\partial \mathrm{c}}{\partial \mathrm{t}} + \boldsymbol{u}\cdot\nabla \mathrm{c} = \frac{\dot{\mathrm{m}}}{\rho_{\mathrm{g}}} \tag{12}$$

where the parameter c is the volume fraction of the vapour, which varies between 0 and 1.

In addition, after obtaining the level set function, the density ρ and viscosity η are given by:

$$\rho(\phi) = \rho_g H(\phi) + \rho_l(1-H(\phi)) \tag{13}$$

$$\eta(\phi) = \eta_g H(\phi) + \eta_l(1-H(\phi)) \tag{14}$$

where $H(\phi)$ is smooth Heaviside function and can be written as:

$$H(\phi) = \begin{cases} 0 & \text{when } \phi < -s \\ \frac{1}{2}\left[1 + \frac{\phi}{s} + \frac{1}{\pi}\sin\left(\frac{\pi\phi}{s}\right)\right] & \text{when } |\phi| < s \\ 1 & \text{when } \phi > s \end{cases} \tag{15}$$

Computational Setup

Description of the Physical Problem

Figure 2 is a schematic of a microchannel. The width and the length of the channel are equal to 0.2 mm and 3 mm, respectively. The liquid enters from the left boundary and flows out from the right boundary. The bubble core is placed on the bottom wall at the initial moment. Properties of water and vapor at 1 atm were used in our simulation, as shown in Table 1. The bottom wall of the microchannel is heated at constant temperature, and the top wall is adiabatic. The wall contact angle is 40°.

Initial and Boundary Conditions

In order to provide a reasonable initial temperature field and velocity field, we first calculate the single-phase liquid flow until it reaches steady state, and then take the temperature field and velocity field under steady state as the initial conditions for two-phase flow simulation.

The boundary conditions on the bottom and top wall are no slip boundary conditions. The bottom wall is explicitly defined at a constant temperature and the top wall is adiabatic. The conditions are mentioned as follows:

At $y = 0$ (bottom boundary),

$$u = v = 0 \text{ and } T = T_{sat} + \Delta T_{\text{sup}}$$

and $y = H$ (top boundary),

$$u = v = 0, k/C_p = 0.$$

Outflow condition is incorporated at the right boundary and velocity inlet condition is incorporated at the left boundary, as shown the following expresses.

At $x = 0$ (left boundary),

$$u = u_0; v = 0; T = T_{sat}$$

and $x = L$ (right boundary),

$$\frac{\partial u}{\partial x} = \frac{\partial v}{\partial x} = \frac{\partial T}{\partial x} = 0.$$

Grid Independence Study

In order to get reasonable calculation results, the mesh independency study is required. Four different grid sizes of 6.67 μm, 5 μm, 4 μm and 3.33 μm were adopted to simulate the growth of a single bubble. Figure 3 shows the terminal shape of the phase interface obtained under different grid sizes at 1.5 ms, indicating that the shape of the phase interface has no significant change when the gird is finer than 4 μm. Moreover, the difference between the average diameters of the bubbles with the grid size of 4 μm and 3.33 μm was less than 1%. According to the above results, the grid resolution 4 μm has the adequate numerical accuracy and is adopted in the rest of our simulations.

Verification of the Present Numerical Model

The experimental results conducted by Mukherjee et al. (2011) were used to verify the accuracy of the numerical model introduced in this paper. Mukherjee et al. (2011) measured

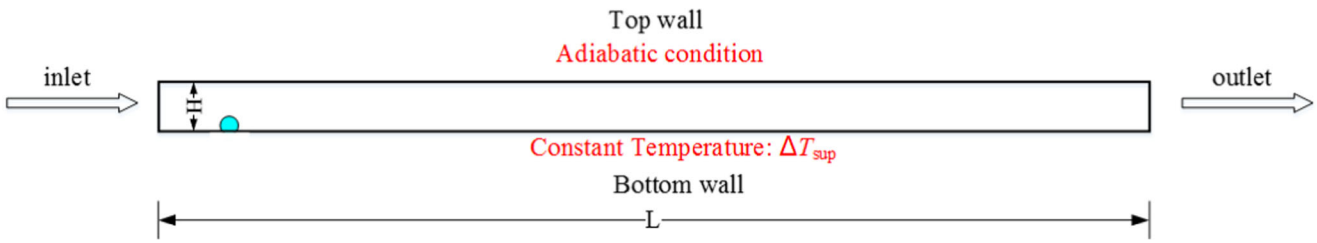

Fig. 2 Schematic of the computational domain

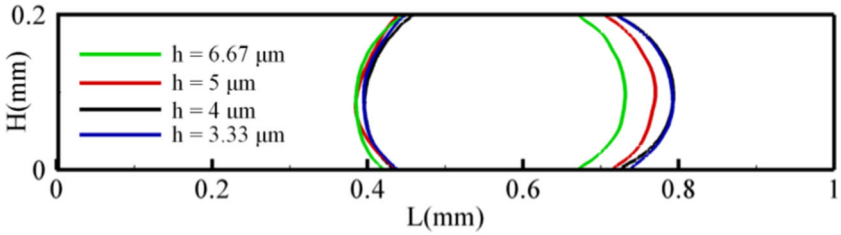

Fig. 3 Interface positions obtained in different grid sizes

the growth rate of a single bubble in a microchannel by experimental method. A single bubble grows from the bottom wall of the microchannel until the entire channel is fully filled. Their experimental conditions are shown including: (1) the width of the channel is equal to 229 μm; (2) the superheat of both the initial and inlet temperature is equal to 2 K; (3) the superheat of the bottom wall is equal to 2.1 K; (4) the wall contact angle is 30°; (5) the top wall is adiabatic; (6) the Reynolds number of the inlet liquid is 100.

Figure 4 shows the change of the bubble equivalent diameters over time obtained by our simulations, and also gives the simulation results of Mukherjee et al. (2011) and Ling et al. (2015). The three simulation results are compared with the experimental results of Mukherjee et al. (2011), which indicates that the bubble growth rate calculated by the three simulations is basically the same as the experimental results and the calculated results in this paper are more similar to the experimental results. The comparison demonstrates the reliability of our numerical methods.

Results and Discussion

Effect of Reynolds Number

The position, shape, velocity vector and temperature field distribution of the bubble at 0.9 ms for the wall superheat of 5 K are shown in Fig. 5. In Fig. 5, the bubble fills completely the channel at 0.9 ms when Re = 100, then grows along the axis direction. The larger the Reynolds number is, the earlier the bubble fills the entire channel. The morphology of the bubble will be different with an increase in Reynolds number at the same time. When Re is small (Re < 600), there is no elongated bubble zone mentioned by (Thome 2004; Thome et al. 2004). When Re = 600, a thin liquid layer is formed between the bubble and the wall, and the elongated bubble zone appears. The dynamics and heat transfer characteristics of the elongated bubble will be discussed in detail later. As can be seen from the temperature field distribution in Fig. 5, as the Reynolds number increases, the thickness of the thermal boundary layer decreases, leading to an increase in the temperature gradient near the heated wall. And then the heat flux increases according to Fourier law of heat conduction, indicating that the heat transfer performance can be enhanced with an increase in Reynolds number.

Figure 6a and b show the effect of Reynolds number on the bubble growth rate. Figure 6a depicts the effect of Reynolds number on the bubble volume and Fig. 6b shows the effect of Reynolds number on the bubble equivalent diameter. There is a negligible difference in the bubble volume for Re = 50 and Re = 100, and so is the bubble equivalent diameter. However, the bubble growth rate increases with an increase in the Reynolds number comparing the trends of bubble growth rate at Re = 100, Re = 200, Re =400 and Re = 600. As known in Eq. (1), the bubble growth rate represents the intensity of phase chance. Therefore, increasing Reynolds number can enhance the intensity of phase chance.

Nu_0 and Nu are the space-averaged Nusselt number of single-phase flow and boiling flow, respectively. Nu/ Nu_0

Table 1 Properties of liquid and vapor phases of water at 1 atm

	Liquid	Vapor
Density(kg/m^3)	958.0	0.6
Dynamic viscosity(kg/m·s)	2.82×10^{-4}	12.3×10^{-6}
Thermal conductivity(W/m·K)	0.683	0.025
Thermal capacity(J/kg·K)	4200.0	2100.0
Surface tension coefficient(N/m)	0.059	
Latent heat(J/kg)	2.257×10^6	

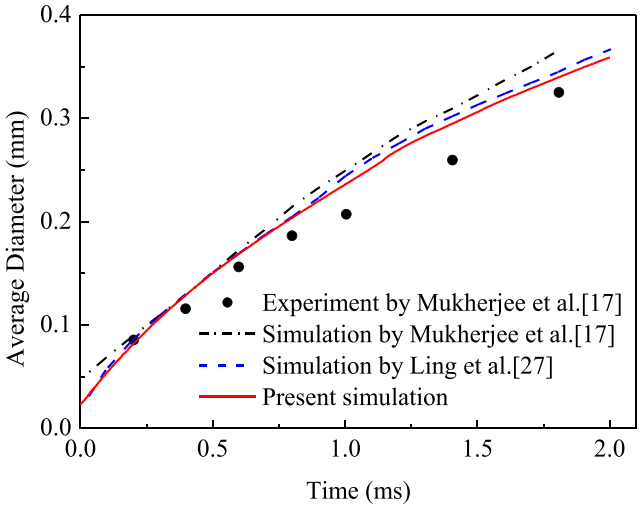

Fig. 4 Bubble growth rate in different studies and the comparison with the experimental result by Mukherjee et al. (2011)

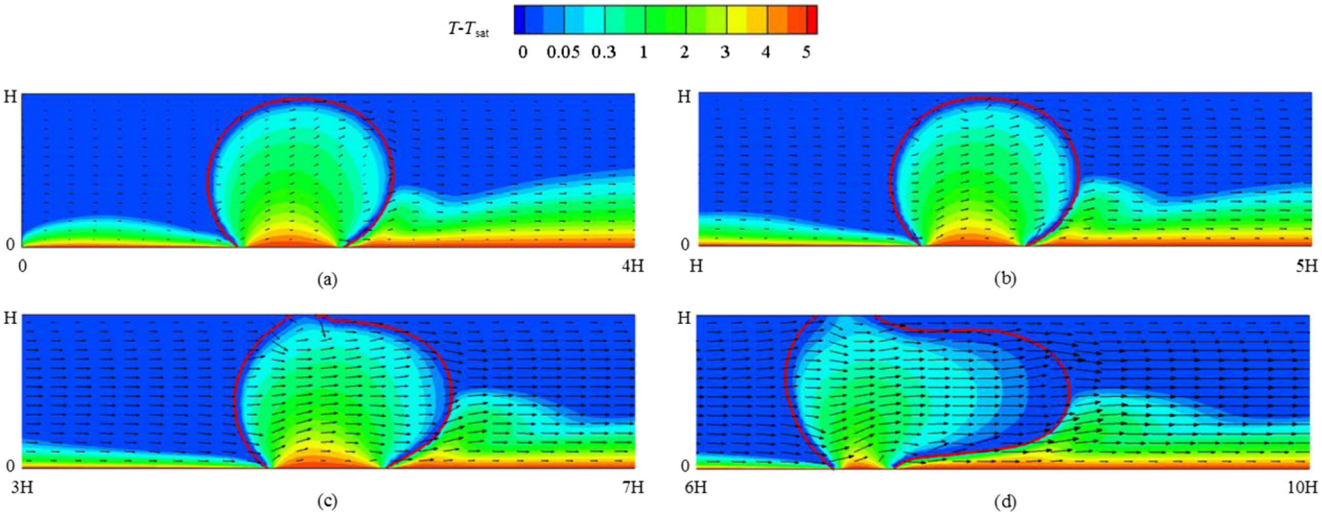

Fig. 5 Bubble shapes and temperature contours for a wall superheat of 5 K and different Re at 0.9 ms, for **a** Re = 100 **b** Re = 200 **c** Re = 400 and **d** Re = 600. The red solid line refers to the interface

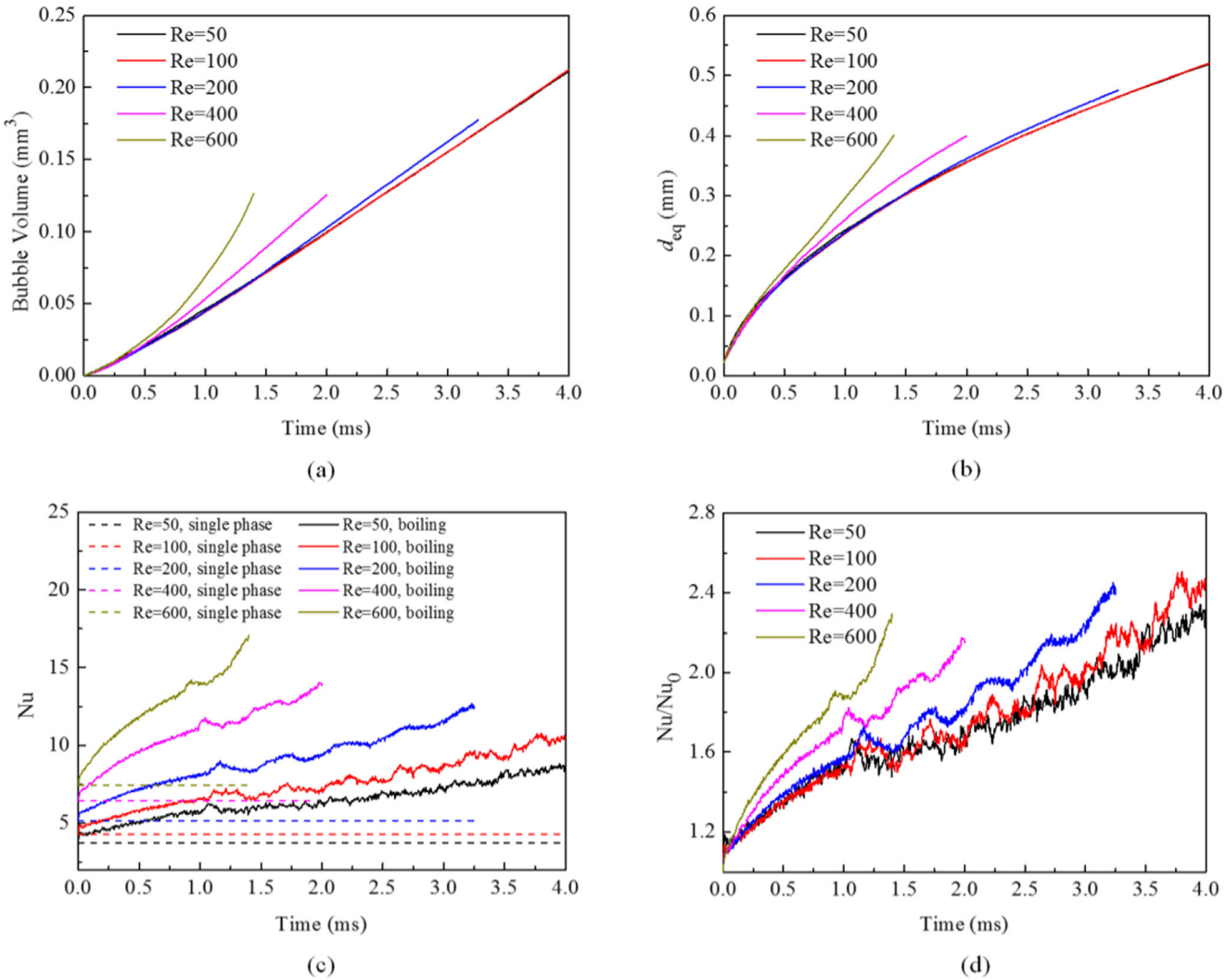

Fig. 6 Effect of Reynolds number on temporal variation of **a** bubble volume, **b** bubble equivalent diameter, space averaged **c** Nusselt Number and **d** $\Delta Nu/Nu_0$ for bottom wall for a wall superheat of 5 K

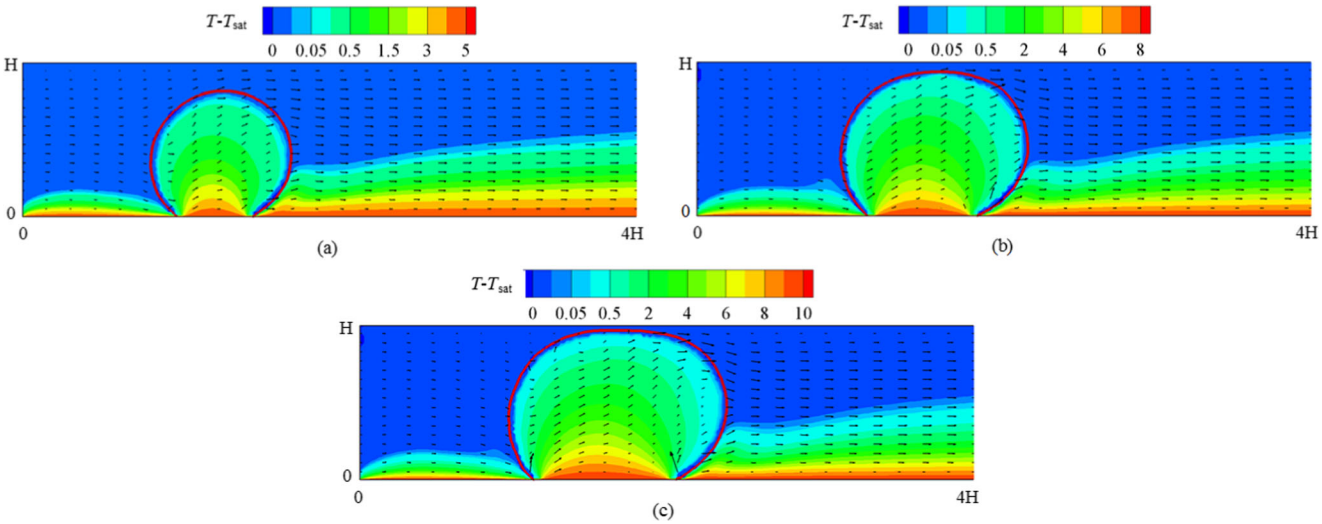

Fig. 7 Bubble shapes and temperature contours for Re = 100 and different wall superheats of **a** 5 K **b** 8 K **c** 10 K at 0.6 ms. The red solid line refers to the interface

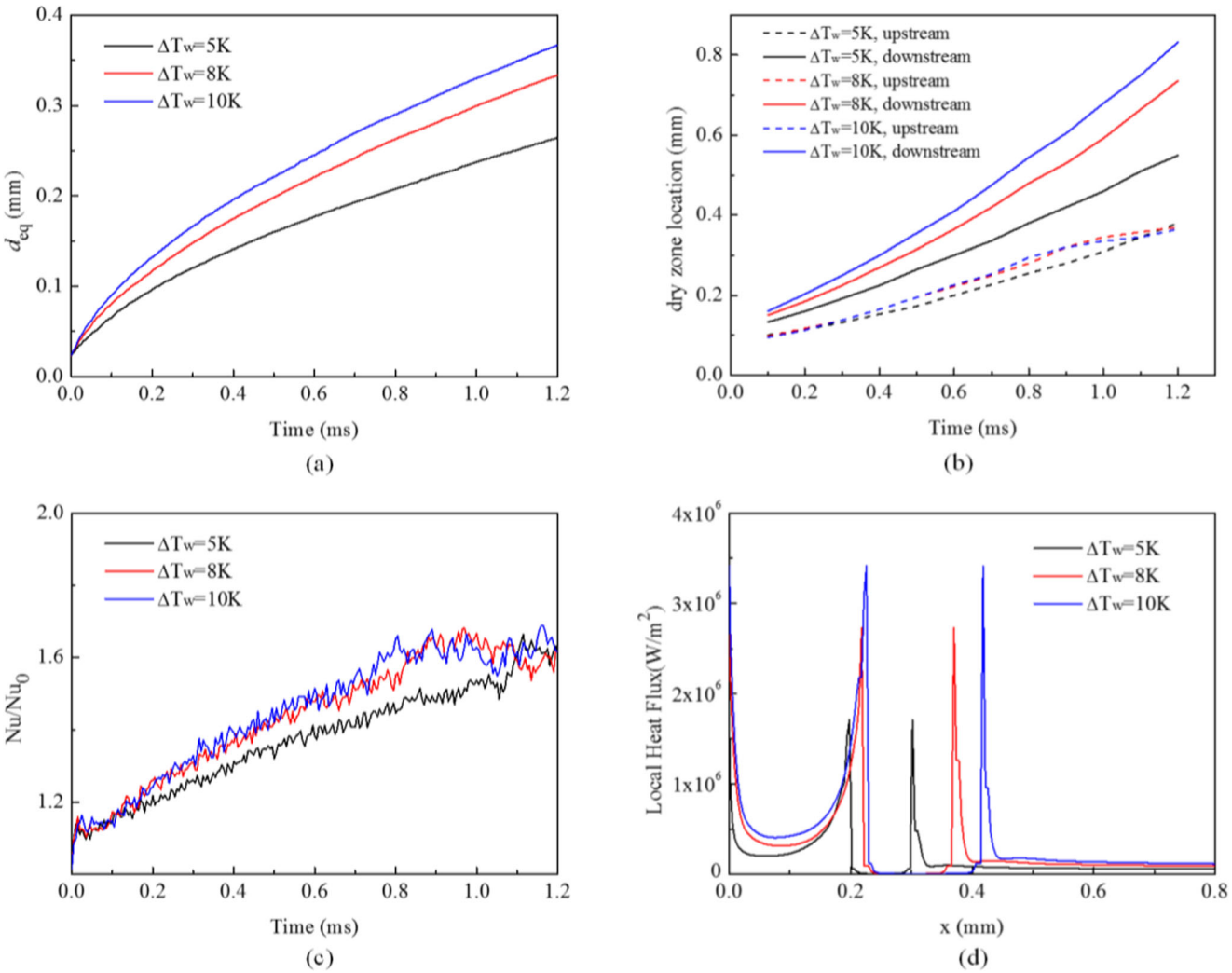

Fig. 8 Effect of wall superheat on temporal variation of **a** bubble equivalent diameter, **b** upstream and downstream dry zone locations and **c** space averaged Nusselt Number; and axial variation of **d** local heat transfer for bottom wall at 0.6 ms.

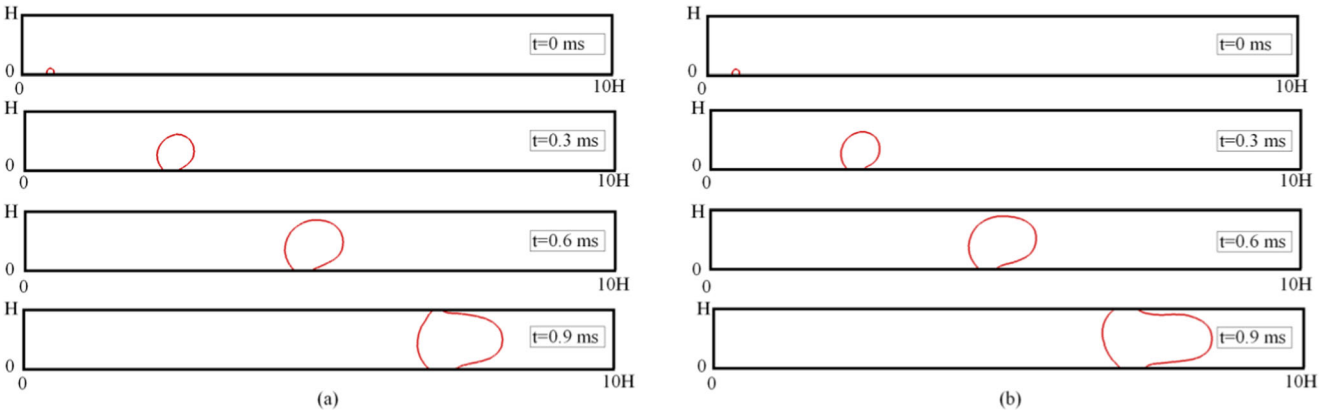

Fig. 9 Interface evolution for Re = 600 and different wall superheat of (a) 4 K and (b) 5 K

represents the enhanced heat transfer intensity due to phase change. Figure 6c and d show the effect of Reynolds number on the space-averaged Nusselt number and Nu/Nu_0 for heated wall during boiling flow in microchannels, respectively. It can be noted that increasing Reynolds could increase not only the space-averaged Nusselt number but also Nu/Nu_0, indicating that with the increase in Reynolds number, the convection heat transfer between the fluids and heated wall and the phase chance intensity are both enhanced.

Effect of Wall Superheat

The influence of wall superheat on the evolution of the bubble, velocity field, temperature field and heat transfer characteristics in a microchannel is presented in this section. The wall superheat plays a very crucial role in determining the dynamics of fluid flow and heat transfer. It affects the quantity of heat input from the wall and then determines the critical heat flux (CHF) and boiling instabilities. It is essential to study the effect of wall superheat on the bubble dynamics and heat transfer characteristics in order to understand deeply the boiling mechanism in microchannels. Figure 7 displays bubble shapes, velocity vector and temperature contours for Re = 100 and different wall superheats. With an increase in the wall superheat, the bubble size and bubble elongation length along the flow direction increase. The dry zone length (i.e., the contact length between the bubble and the heated wall) also increases with an increase in the wall superheat. Based on the mass conservation eq. (1), the magnitude of velocity downstream is higher than that upstream due to the increasing bubble volume.

Figure 8a shows the effect of wall superheat on temporal variation of the equivalent bubble diameters. With an increase in wall superheat, more heat transfers from the heated wall to the bubble, leading to an increase in the bubble equivalent diameters and bubble growth rate. The result is clearly presented in Fig. 8a. Figure 8b depicts the upstream and downstream dry zone locations of the vapour bubble with time. The dotted lines in the figure represent the upstream location of the bubble dry zone and the solid lines represent the downstream location of the bubble dry zone. With an increase in wall superheat, there is a little difference in the upstream location of the bubble dry zone, however significant difference in the downstream location of the bubble dry zone is observed. This is because, with an increase in wall superheat, more heat through the heated wall cause the larger velocity of downstream interface of the bubble.

Figure 8c presents the temporal variation in Nu/Nu_0 (i.e., the ratio of the space averaged Nusselt number between boiling and single liquid flow) at the heated wall. As an increase in wall superheat from 5 K to 8 K, there is a little increase in Nu/Nu_0 and no significant difference in Nu/Nu_0 for 8 K and 10 K is observed. Increasing wall superheat not only produces the higher heat flux, but also causes larger temperature difference. The combined effect of the two results led to an insignificant enhancement of heat transfer. Figure 8d shows the axial variation of the local heat transfer for heated wall at 0.6 ms. With an increase in wall superheat, the local heat flux for

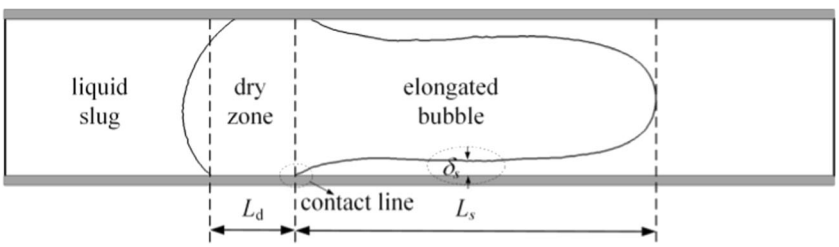

Fig. 10 Schematic of elongated bubble in microchannel

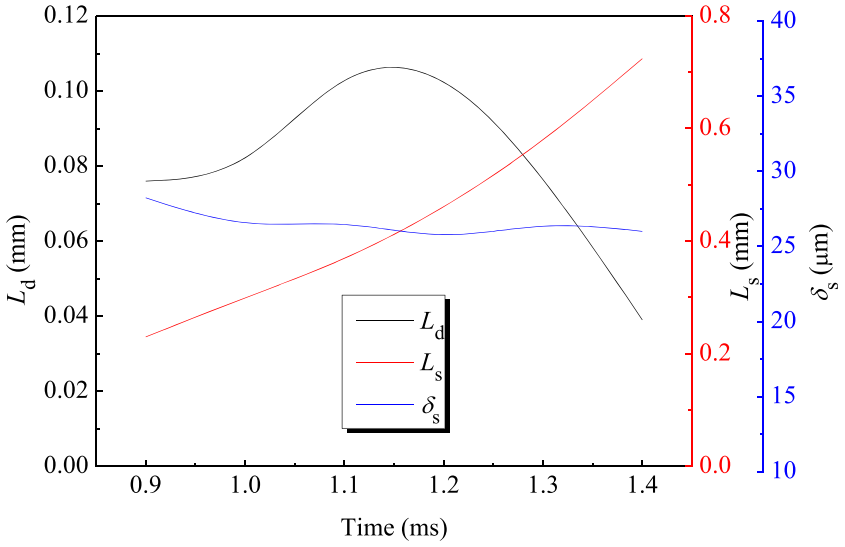

Fig. 11 Temporal variation in L_s, L_d and δ_s, for a wall superheat of 5 K and Re = 600

the heated wall along the flow direction at 0.6 ms increases. Near the upstream and downstream interface, the maximum heat flux is discovered due to the presence of the thin liquid film near the triple-phase contact line. The maximum heat flux increases with an increase in wall superheat because of higher temperature gradient.

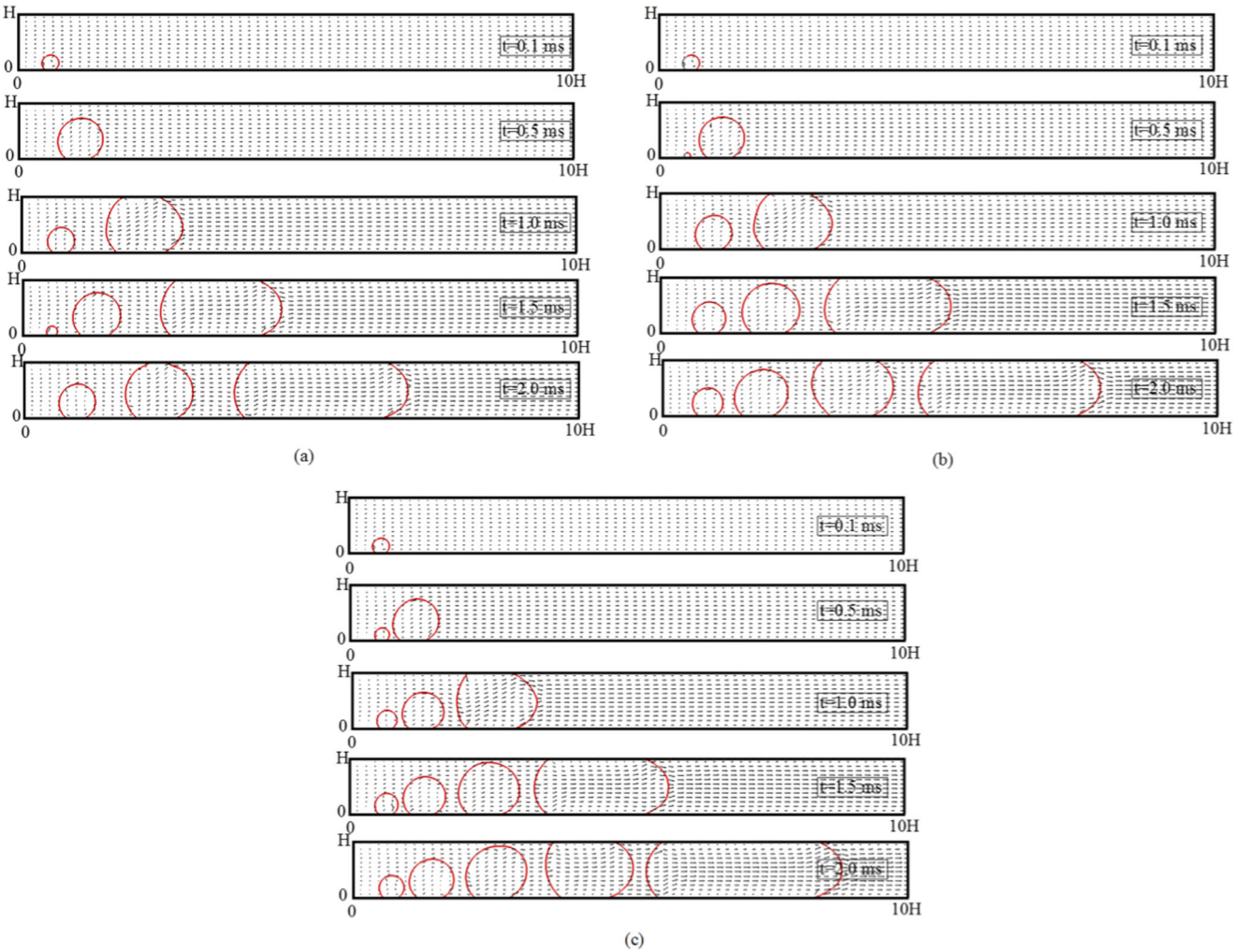

Fig. 12 Interface evolution for a wall superheat of 5 K, Re = 100 and different bubble waiting time of **a** 0.5 ms, **b** 0.3 ms and **c** 0.2 ms.

Bubble Dynamics at Re = 600

As mentioned above, when Re = 600, the morphology of the bubble is different significantly from that of low Reynolds number. Figure 9 shows the effect of wall superheat on the interface evolution of the bubble in the microchannel when Re = 600. At the initial stage of the bubble growth, the bubble grows on the heating wall and slides downstream along the flow direction. When the bubble grows to a certain size and then starts to touch the top wall. The bubble fills the entire channel and begins to stretch along the axis of the channel. Three zones mentioned by (Thome 2004; Thome et al. 2004) appear in the microchannel, namely liquid slug zone, elongated bubble zone and dry zone. As an increase in wall superheat, the longitudinal elongation of the bubble increases, however the vapour contact with the heated wall decreases. Two kinds of thin liquid layers have appeared in the simulation results in this paper. The first type of thin liquid layer is located near the three-phase contact line. The second type of thin liquid layer refers to the liquid area between the phase interface and the wall surface when the bubble interface is close to the wall surface, as shown in Fig. 10. Fig. 10 also gives the definition of the stretch length L_s, the contact length between the bubble and the bottom wall (i.e., the dry zone length) L_d and the thickness of the second type of the thin liquid layer δ_s. Figure 11 shows the variation of L_s, L_d and δ_s over time. In the process of longitudinal elongation of the bubble, the stretch length L_s of the elongated bubble along the flow direction increases gradually. Because of the continual heat transportation from the bottom wall, the volume of the bubble increases gradually and L_d increases gradually. When the bubble is stretched to a certain size, there is a trend to break away from the bottom wall, and then the L_d decreases gradually. In the process of longitudinal elongation of the bubble, δ_s is basically unchanged, which is about 26 μm for a wall superheat of 5 K.

Multiple Bubbles Dynamics and Heat Transfer

The bubble waiting time, which refers to the time between the bubble departing a certain position and the formation of the next bubble, is one of the most important parameters involved in bubble dynamics and heat transfer. The effect of bubble waiting time on bubble dynamics and heat transfer in a microchannel is presented in this section, which considers static bubble waiting time of 0.5 ms, 0.3 ms and 0.2 ms. Figure 12 shows the effect of bubble waiting time on the interface evolution and velocity vectors throughout the domain for a wall superheat of 5 K and Re = 100. It is necessary to note that Fig. 12 shows only part of the computational domain, not all of it. At the time of 2.0 ms, when the bubble waiting time is 0.5 ms, 0.3 ms and 0.2 ms, the number of bubbles in the microchannel is 3, 4 and 5, respectively. With a decrease in bubble waiting time, more bubbles are formed in the same time period, and the flow pattern in the microchannel is plug flow. When a new bubble is formed, the velocity downstream of the bubble increases. On the same section of the microchannel, an increase in the velocity in the liquid downstream of the bubble can be observed with a decrease in bubble waiting time.

Figure 13a plots the effect of bubble waiting time on temporal variation of the space-averaged Nusselt number for the heated wall with time. As a decrease in bubble waiting time, the space-averaged Nusselt number for the heated wall increases. Figure 13b shows the axial variation of local heat flux on the heated wall for bubble waiting time of 0.5 ms at 2 ms. The inset figure in Fig. 13b shows the bubble shape and temperature contour at 2 ms. It can be seen from the figure that the thin film evaporation of liquid film occurs between the bubble and the heated wall and the local heat flux of the liquid film takes up a large proportion in

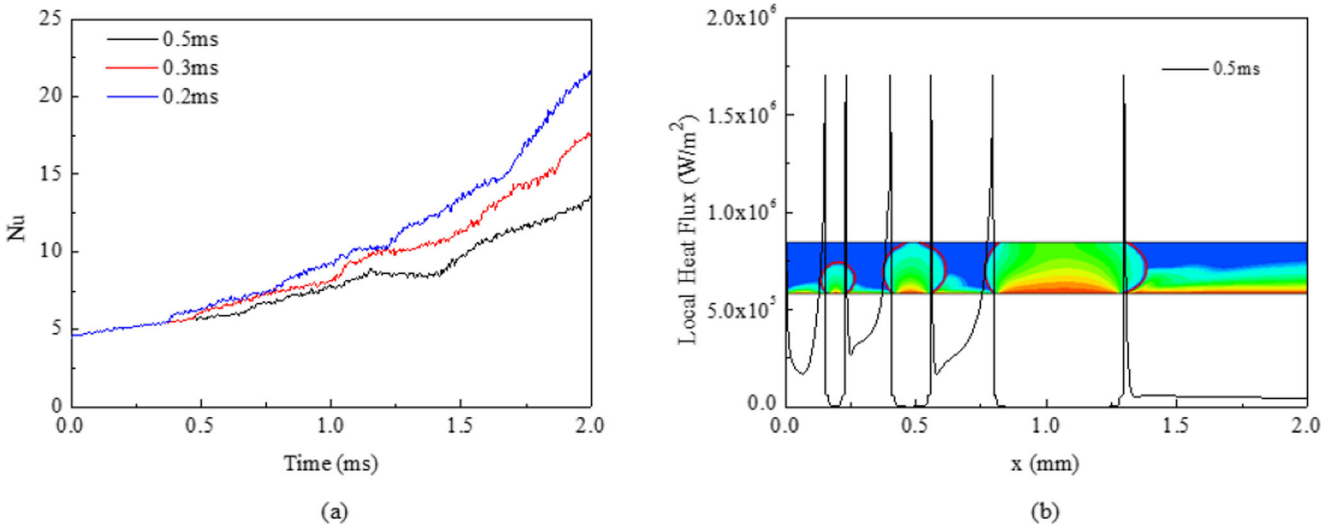

Fig. 13 **a** the effect of bubble wait time on temporal variation of the space averaged Nusselt number for the heated wall; **b** the axial variation of local heat flux on the heated wall for bubble waiting time of 0.5 ms at 2 ms. Inset figure in figure (b) shows the bubble shape and temperature contour at 2 ms.

the total heat flux. This shows that the thin film evaporation of liquid film is the main heat transfer mechanism of the plug flow. Due to the influence of the convection evaporation of the liquid film, the local heat flux for the heated wall between the bubbles also increases significantly. In addition, as a decrease in bubble waiting time, the distance between bubbles decreases, while the local heat flux for the heated wall between bubbles increases more dramatically. More importantly, with an increase in the number of bubbles, the number of liquid film between the bubble and the heated wall increases, which could enhance the total heat flux.

Conclusions

In this paper, the VOSET interface tracking method was used to simulate the growth and heat transfer characteristics of single bubble and multiple bubbles during boiling flow in a microchannel with heated bottom wall. The following conclusions could be obtained.

(1) The influence of Reynolds number and wall superheat on the growth and heat transfer characteristics of single bubble was studied. Increasing Reynolds number not only enhances the convection heat transfer between the fluids and the wall but also strengthens the phase change intensity. With an increase in wall superheat, bubble growth rate increases, however there is an insignificant enhancement of heat transfer.

(2) Different Reynolds number of the inlet fluid lead to different morphology of the bubble in the microchannel. When Re = 600, a thin liquid layer was formed between the bubble and the wall, and obvious elongated bubble zone appeared. In the elongation process of the elongated bubble along the axis, the stretching length L_s gradually increases, and the contact length L_d between the bubble and the heating wall surface presents a trend of first increasing and then decreasing. The thickness of the second type of thin liquid layer δ_s is basically unchanged.

(3) More importantly, the influence of bubble waiting time on heat transfer characteristics and bubble growth was established. With a decrease in bubble waiting time, more bubbles emerge, and the flow pattern in the microchannel is the plug flow. The decreasing bubble waiting time increases the number of thin liquid film between the bubble and the heated wall, leading to a larger proportion of thin film evaporation in total heat transfer, which can enhance the heat transfer performance.

Acknowledgements The authors wish to acknowledge the support of the National Basic Research Program of China (973 Program) (Grant, No. 2015CB251502) and the National Natural Science Foundation of China (U1738105).

References

Agostini, B., Fabbri, M., Park, J.E., Wojtan, L., Thome, J.R., Michel, B.: State of the Art of High Heat Flux Cooling Technologies. Heat Transfer Engineering. **28**, 258–281 (2007)

Agostini, B., Revellin, R., Thome, J.R.: Elongated bubbles in microchannels. Part I: Experimental study and modeling of elongated bubble velocity. Int. J. Multiphase Flow. **34**, 590–601 (2008)

Arcanjo, A.A., Tibiriçá, C.B., Ribatski, G.: Evaluation of flow patterns and elongated bubble characteristics during the flow boiling of halocarbon refrigerants in a micro-scale channel. Exp. Thermal Fluid Sci. **34**, 766–775 (2010)

Arias, S., Ruiz, X., Casademunt, J., Ramírez-Piscina, L., González-Cinca, R.: Experimental Study of a Microchannel Bubble Injector for Microgravity Applications. Microgravity Science and Technology. **21**, 107–111 (2008)

Balasubramanian, P., Kandlikar, S.G.: Experimental Study of Flow Patterns, Pressure Drop and Flow Instabilities in Parallel Rectangular Minichannels. Heat Transfer Engineering. **26**, 20–27 (2005)

Baldassari, C., Marengo, M.: Flow boiling in microchannels and microgravity. Prog. Energy Combust. Sci. **39**, 1–36 (2013)

Brackbill, J.U., Kothe, D.B., Zemach, C.: A continuum method for modeling surface tension. J. Comput. Phys. **100**, 335–354 (1992)

Dhir, V.K., Warrier, G.R., Aktinol, E., Chao, D., Eggers, J., Sheredy, W., Booth, W.: Nucleate Pool Boiling Experiments (NPBX) on the International Space Station. Microgravity Science and Technology. **24**, 307–325 (2012)

Guo, Z., Fletcherl, D.F., Haynes, B.S.: A Review of Computational Modelling of Flow Boiling in Microchannels. The Journal of Computational Multiphase Flows. **6**, 79–110 (2014)

Harirchian, T., Garimella, S.V.: A comprehensive flow regime map for microchannel flow boiling with quantitative transition criteria. Int. J. Heat Mass Transf. **53**, 2694–2702 (2010)

Huh, C., Choi, C.W., Kim, M.H.: Elongated bubble behavior during flow boiling in a microchannel. J. Mech. Sci. Technol. **21**, 1819–1827 (2007)

Hussien, A.A., Abdullah, M.Z., Al-Nimr, M.d.A.: Single-phase heat transfer enhancement in micro/minichannels using nanofluids: Theory and applications. Appl. Energy. **164**, 733–755 (2016)

Jafari, R., Okutucu-Özyurt, T.: Numerical simulation of flow boiling from an artificial cavity in a microchannel. Int. J. Heat Mass Transf. **97**, 270–278 (2016)

Kandlikar, S.G.: Fundamental issues related to flow boiling in minichannels and microchannels. Exp. Thermal Fluid Sci. **26**, 389–407 (2002)

Karayiannis, T.G., Mahmoud, M.M.: Flow boiling in microchannels: Fundamentals and applications. Appl. Therm. Eng. **115**, 1372–1397 (2017)

Katiyar, G., Karagadde, S., Saha, S.K., Sharma, A.: Numerical modelling of bubble growth in microchannel using Level Set Method. Int. J. Heat Mass Transf. **101**, 719–732 (2016)

Kattan, N., Thome, J.R., Favrat, D.: Flow boiling in horizontal tubes: Part 1 - Development of a diabatic two-phase flow pattern map. Journal of Heat Transfer-Transactions of the Asme. **120**, 140–147 (1998a)

Kattan, N., Thome, J.R., Favrat, D.: Flow boiling in horizontal tubes: Part 2 - New heat transfer data for five refrigerants. Journal of Heat Transfer-Transactions of the Asme. **120**, 148–155 (1998b)

Kattan, N., Thome, J.R., Favrat, D.: Flow boiling in horizontal tubes: Part 3 - Development of a new heat transfer model based on flow pattern. Journal of Heat Transfer-Transactions of the Asme. **120**, 156–165 (1998c)

Kim, S.M., Mudawar, I.: Review of databases and predictive methods for heat transfer in condensing and boiling mini/micro-channel flows. Int. J. Heat Mass Transf. **77**, 627–652 (2014)

Konishi, C., Mudawar, I.: Review of flow boiling and critical heat flux in microgravity. Int. J. Heat Mass Transf. **80**, 469–493 (2015)

Krishnan, S., Garimella, S.V., Chrysler, G.M., Mahajan, R.V.: Towards a thermal Moore's law. IEEE Trans. Adv. Packag. **30**, 462–474 (2007)

Kuznetsov, V.V., Shamirzaev, A.S.: Flow Boiling Heat Transfer in Two-Phase Micro Channel Heat Sink at Low Water Mass Flux. Microgravity Science and Technology. **21**, 305–311 (2009)

Lee, W., Son, G.: Bubble Dynamics and Heat Transfer During Nucleate Boiling in a Microchannel. Numerical Heat Transfer, Part A: Applications. **53**, 1074–1090 (2008)

Ling, K., Son, G., Sun, D.L., Tao, W.Q.: Three dimensional numerical simulation on bubble growth and merger in microchannel boiling flow. Int. J. Therm. Sci. **98**, 135–147 (2015)

Luo, Y., Zhang, J., Li, W., Sokolova, E., Li, Y., Minkowycz, W.J.: Numerical investigation of the bubble growth in horizontal rectangular microchannels. Numerical Heat Transfer, Part A: Applications. **71**, 1175–1188 (2017)

Ma, R., Wu, Y.-t., Du, C.-x., Chen, X., Ma, C.-f., Yan, S.: Experimental Study of Weightless Effect on Small Vapor Compression Heat Pump. Microgravity Science and Technology. **30**, 977–985 (2018)

Magnini, M., Pulvirenti, B., Thome, J.R.: Numerical investigation of hydrodynamics and heat transfer of elongated bubbles during flow boiling in a microchannel. Int. J. Heat Mass Transf. **59**, 451–471 (2013a)

Magnini, M., Pulvirenti, B., Thome, J.R.: Numerical investigation of the influence of leading and sequential bubbles on slug flow boiling within a microchannel. Int. J. Therm. Sci. **71**, 36–52 (2013b)

Mukherjee, A.: Contribution of thin-film evaporation during flow boiling inside microchannels. Int. J. Therm. Sci. **48**, 2025–2035 (2009)

Mukherjee, A., Kandlikar, S.G.: Numerical simulation of growth of a vapor bubble during flow boiling of water in a microchannel. Microfluid. Nanofluid. **1**, 137–145 (2005)

Mukherjee, A., Kandlikar, S.G., Edel, Z.J.: Numerical study of bubble growth and wall heat transfer during flow boiling in a microchannel. Int. J. Heat Mass Transf. **54**, 3702–3718 (2011)

Revellin, R., Agostini, B., Ursenbacher, T., Thome, J.R.: Experimental investigation of velocity and length of elongated bubbles for flow of R-134a in a 0.5mm microchannel. Exp. Thermal Fluid Sci. **32**, 870–881 (2008)

Sun, D.L., Qu, Z.G., He, Y.L., Tao, W.Q.: An Efficient Segregated Algorithm for Incompressible Fluid Flow and Heat Transfer Problems—IDEAL (Inner Doubly Iterative Efficient Algorithm for Linked Equations) Part I: Mathematical Formulation and Solution Procedure. Numerical Heat Transfer, Part B: Fundamentals. **53**, 1–17 (2008)

Sun, D.L., Tao, W.Q.: A coupled volume-of-fluid and level set (VOSET) method for computing incompressible two-phase flows. Int. J. Heat Mass Transf. **53**, 645–655 (2010)

Thome, J.R.: Boiling in microchannels: a review of experiment and theory. Int. J. Heat Fluid Flow. **25**, 128–139 (2004)

Thome, J.R., Dupont, V., Jacobi, A.M.: Heat transfer model for evaporation in microchannels. Part I: presentation of the model. Int. J. Heat Mass Transf. **47**, 3375–3385 (2004)

Tibiriçá, C.B., Ribatski, G.: Flow boiling in micro-scale channels – Synthesized literature review. Int. J. Refrig. **36**, 301–324 (2013)

Udaykumar, H.S., Mittal, R., Shyy, W.: Computation of Solid–Liquid Phase Fronts in the Sharp Interface Limit on Fixed Grids. J. Comput. Phys. **153**, 535–574 (1999)

Wan, S.-X., Zhao, J.-F.: Pool Boiling in Microgravity: Recent Results and Perspectives for the Project DEPA-SJ10. Microgravity Science and Technology. **20**, 219–224 (2008)

Wang, T., Li, H.X., Zhang, Y.F., Han, W., Sheng, T.Y., Zhang, W.Q.: Numerical Simulation of Two-Phase Flows Using 3D-VOSET Method on Dynamically Adaptive Octree Grids. 2014 22nd International Conference on Nuclear Engineering, Prague (2014)

Wang, Y., Wang, Z.G.: An overview of liquid–vapor phase change, flow and heat transfer in mini- and micro-channels. Int. J. Therm. Sci. **86**, 227–245 (2014)

Wu, W., Zhang, M.T., Zhang, X.B., Xia, J.J., Wen, S.Z., Wang, Z.R., He, Z.H., Huang, Z.C.: Experimental Investigation of Flow Boiling in Parallel Mini-channels. Microgravity Science and Technology. **27**, 273–279 (2015)